Efficient Integrated Multimode Amplifiers for Scalable Long-Haul SDM Transmission

Hrishikesh Srinivas, *Member, IEEE*, Oleksiy Krutko, and Joseph M. Kahn, *Fellow, IEEE*

***Abstract*—Scaling up cable capacity in a power- and cost-efficient manner is a goal of spatial-division multiplexing (SDM) in long-haul optical communication systems. Integration is a key to scaling SDM beyond the parallel single-mode fiber paradigm. Multicore or multimode fiber systems promise higher integration, but native multicore or multimode amplifiers pose challenges in efficient coupling of pump light into the amplifier, and in control of mode-dependent gain (MDG). We propose an integrated multimode amplifier design for signals in six spatial modes (12 spatial and polarization modes) that relies on excitation of only four pump spatial modes at 980 nm. Simulations of an exemplary amplifier predict a relatively flat gain above 10 dB, noise figure below 5 dB, and MDG standard deviation below 0.1 dB over the C-band (1530–1565 nm), with a power-conversion efficiency close to 30%. Key design features include a graded-index multimode fiber amplifier with optimized ring erbium doping profile, length and pump mode powers; and a cascade of wavelength- and mode-selective couplers that efficiently couples four pump diodes to four pump modes, while passing signal modes with minimal loss. Our design approach, which uses fewer pump diodes per signal mode than parallel single-mode systems, may provide an option for efficient, economical scaling of SDM long-haul systems.**

***Index Terms*—Couplers, optical amplifiers, optical fiber communication, space division multiplexing, system integration.**

I. Introduction

POWER-LIMITED long-haul optical communication systems exploit power-efficient spatial-division multiplexing (SDM) to deliver higher cable capacities to meet ever-increasing worldwide demand. In current systems using parallel single-mode fibers (SMFs), SDM optimizes system power efficiency, defined as capacity per unit power, by transmitting through a larger number of fiber pairs at lower power and data rate per fiber, thereby maximizing cable capacity subject to feed-power constraints [1], [2], [3], [4].

Alternate designs using coupled-core multicore fiber (CC-MCF) or multimode fiber (MMF) can potentially enhance integration and scalability in SDM systems, improving their power and cost efficiencies [5]. Beneficial SDM transmission fiber characteristics have been identified and studied [6], [7], [8], including ultra-low loss [9], large effective area and low nonlinearity [10], [11], [12], and strong, random mode coupling reducing the impact of transmission fiber group delay (GD) spread and amplifier mode-dependent gain (MDG) [13], [14], [15]. Comparison between MMF and CC-MCF transmission fibers is ongoing, with CC-MCFs showing better performance metrics so far [16].

In tandem, research has addressed the requirements for MMF and CC-MCF amplifiers to support efficient SDM transmission: gain sufficient to overcome span loss, low noise figure (NF), low MDG, and high power-conversion efficiency (PCE). In particular, MDG poses greater challenges than the polarization-dependent gain (PDG) encountered in parallel SMF systems. The study [17] quantified the impact of MDG on capacity for various regimes of link signal-to-noise ratio (SNR) evolution and various receiver architectures, and showed that strongly coupled multimode or multicore transoceanic systems require very low MDG to keep capacity losses at tolerably low levels. Apart from the doped fibers themselves, passive components in amplifier nodes, such as pump couplers, should introduce low mode-averaged loss and mode-dependent loss (MDL) for both signal and pump to minimize transmission impairments and maximize power efficiency [18], [19].

Achieving the integration objectives and performance requirements in CC-MCF and MMF amplification remains challenging. Multicore amplification typically relies on complex, lossy fan-out/fan-in networks with single-mode amplifiers or inefficient, cladding-based pumping of multicore amplifiers [20], [21], [22], [23], [24], [25], [26], [27], [28]. Multimode erbium-doped fiber amplifiers (MM-EDFAs) promise integration in SDM systems [29], [30], but have been limited to date by excessive MDG and by higher NFs and lower PCEs than single-mode EDFAs. MDG reduction by optimizing EDF length and doping profile has been studied both in numerical simulations [31], [32], [33] and in experiments [34], [35]. Control of pump modes can reduce MDG, as shown by validated modeling [36], [37], [38]. MDG can be minimized effectively using more complex methods to control pump modes, including phase masks and variable attenuators [39], dynamically optimized spatial light modulators [40] or optimization of numerous pump modes at two pump wavelengths [41]. While each approach has shown promise in reducing MDG, the need remains for power-efficient, cost-effective, integrated solutions satisfying the requirements of long-haul SDM systems.

Manuscript received 18 November 2022; revised 27 January 2023; accepted 28 February 2023. Date of publication 8 March 2023; date of current version 2 August 2023. *(Hrishikesh Srinivas and Oleksiy Krutko contributed equally to this work.) (Corresponding author: Hrishikesh Srinivas.)*

The authors are with the E. L. Ginzton Laboratory, Department of Electrical Engineering, Stanford University, Stanford, CA 94305 USA (e-mail: hrishsri@stanford.edu; oleksiyk@stanford.edu; jmk@ee.stanford.edu).

Color versions of one or more figures in this article are available at https://doi.org/10.1109/JLT.2023.3254305.

Digital Object Identifier 10.1109/JLT.2023.3254305

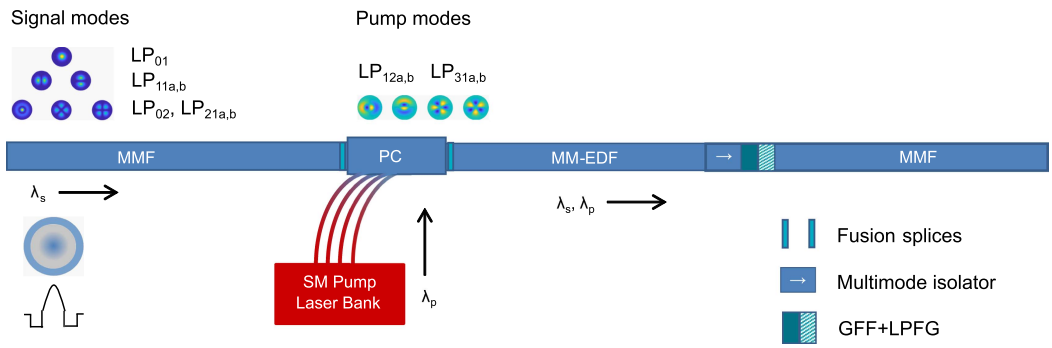

Fig. 1. Schematic of proposed multimode amplifier subsystem. Six signal spatial modes at wavelength λ_s in the C-band are coupled to four pump spatial modes at $\lambda_p = 980\,\mathrm{nm}$ in the pump coupler (PC) and input to the multimode erbium-doped fiber (MM-EDF). The four pump modes are excited by mutually incoherent laser diodes. Components following the MM-EDF include isolator with pump-blocking filter, gain-flattening filter (GFF), and possible mode-scrambling long-period fiber Bragg grating (LPFG). The MMF facet and index profile are shown at left.

In this work, we propose a solution to the challenge of integrated, high-performance MM-EDFAs. We describe a MM-EDFA for six spatial modes based on a graded-index (GI) EDF with optimized ring doping profile, length and pump mode powers. It uses a wavelength- and mode-selective pump coupler (PC) to efficiently couple in four pump modes, while passing the signal modes with minimal loss. We present detailed numerical modeling of the MM-EDFA and the PC, showing that the design promises low MDG, low NF and high PCE over the C-band at signal powers typical for long-haul SDM systems. Although we propose the scheme for a MMF EDFA, where it enables fewer pump modes than signal modes, it may be possible to extend the principle to CC-MCF EDFAs by appropriate redesign of the PC.

The remainder of this paper is organized as follows. Section II describes our multimode amplifier subsystem design and the modeling and optimization methodologies employed. Section III presents the gain, NF, MDG and power efficiency of the optimized MM-EDFAs, and describes the implications of the achieved performance for SDM transmission system design. Section IV addresses fabrication methods to enable the proposed MM-EDFA design, and important remaining challenges for integrating and scaling long-haul systems using MMF or CC-MCF. Section V concludes the paper.

II. Amplifier Subsystem Design

The proposed multimode amplifier subsystem is shown in Fig. 1. Signals in six spatial modes at wavelength λ_s in the C-band are received in a transmission MMF. The outputs of four mutually incoherent pump laser diodes pass through SMFs to the PC, where they couple to four pump spatial modes at $\lambda_p = 980\,\mathrm{nm}$. After amplification in the MM-EDF, signals pass through a multimode isolator with pump-blocking filter [19], a gain-flattening filter (GFF), and possibly a mode-scrambling long-period fiber Bragg grating (LPFG), before exiting through a transmission MMF.

The transmission and amplifier fibers are assumed to have the axially symmetric, trench-assisted GI relative refractive index profile shown in Fig. 2. This profile has an index exponent of $\alpha = 2$, a core diameter of 25 μm, an overall diameter of

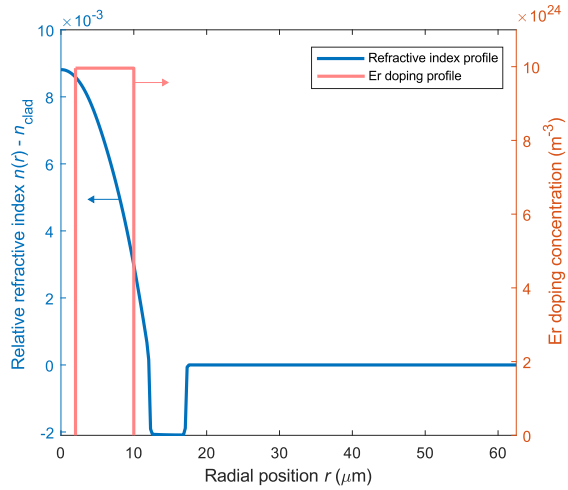

Fig. 2. C-band refractive index profile relative to the cladding index n_{clad} (blue, left ordinate) of the trench-assisted graded-index transmission and amplification MMF with 5 μm-wide trench and 125 μm diameter; and erbium doping profile (pink, right ordinate) with representative inner and outer doping radii at 2 μm and 10 μm.

125 μm, and supports 6 LP spatial modes ($D = 12$ spatial and polarization modes) over the C-band. A 5 μm-wide trench helps minimize micro- and macro-bending losses [42], [43], [44], [45], [46]. The transmission fiber glass would be F-doped silica for ultra-low intrinsic loss [47], [48], [49], [50], [51], and the index contrast assumed here is consistent with pure silica in the center of the core and a maximum of 2.5% wt. F doping in the trench. The mode-averaged chromatic dispersion ranges from 19 to 23 $\mathrm{ps/nm/km}$ as the wavelength varies from 1530 to 1565 nm, while the modal effective areas at 1550 nm range from 120 $\mu\mathrm{m}^2$ for the LP_{01} mode to 240 $\mu\mathrm{m}^2$ for the LP_{02} mode. Simulated guided- and leaky-mode bending losses at signal wavelengths conform to the requirements of standards [52], [53]. We describe modifications to the transmission fiber index profile that minimize GD spread in Section IV-C.

Signals received at the amplifier subsystem are assumed to have undergone a span loss of 10 dB, including transmission fiber, in-line components and coupling losses, thus defining the minimum amplifier gain required.

In the following two subsections, we describe the design of the amplifier, including the erbium doping profile and choice of pump modes, then describe the design of the mode- and wavelength-selective PC.

A. Amplifier Design

In this subsection, we discuss our modeling and optimization methods for MM-EDFAs.

The multimode amplifier is modeled by solving steady-state rate equations for the Er^{3+} ion level populations [54], [55], coupled-mode propagation equations for the evolution of signal and pump mode fields, and power propagation equations for the noise powers along the length of the amplifier. Although signal and pump mode evolution may be modeled using power propagation equations [32], [36], [38], [39], [41], the coupled-mode-field equations ensure accurate computation of gain and MDG. The signal and pump mode fields and associated propagation constants are computed in a radially resolved cylindrical geometry, as in [56]. Our approach follows that of [40] and [57] to capture the effects of mode beating and mode coupling in the MM-EDF, but has two main differences from [40]. First, coupling between pump modes is not assumed negligible, and second, the total local intensity at the pump wavelength is obtained by incoherent addition of the pump modes, assuming pump farming of mutually incoherent laser sources [58]. Amplified spontaneous emission (ASE) noise evolution is modeled using power propagation equations, as in [57]. The EDF absorption and gain cross sections and doping concentration of $9.96 \times 10^{24}\,\mathrm{m}^{-3}$ are those of the single-mode EDF used in the experiments of [1], [59]. These EDF properties are independent of fiber geometry and should be representative of MM-EDFs.

Our primary objective is to minimize the amplifier MDG STD and mode-averaged linear NF, both expressed in dB,[1] while ensuring that the mode- and wavelength-dependent gains are not less than the span attenuation (see Appendix A). We use a particle swarm optimization (PSO) algorithm to optimize the length and inner and outer doping radii of the EDF, along with the powers of the four pump modes in the fourth mode group (LP_{12a}, LP_{12b}, LP_{31a}, LP_{31b}) at pump wavelength $\lambda_p = 980\,\mathrm{nm}$.

The optimizations should favor realizations with mode- and wavelength-dependent gains above yet close to the 10-dB span attenuation, and mode- and wavelength-dependent NFs above yet close to $3\,\mathrm{dB}$, so the objective is formed from the RMS deviations of the two terms from these desired values, with a penalty Φ multiplying the objective for realizations whose computed gains or NFs fall outside the range of desired values. The calculated objective thus takes the form:

$$\Phi\,(G + \theta F)\,, \tag{1}$$

where G is the RMS deviation from the target gain values set to overcome the total span attenuation at all wavelengths for all modes, F is the RMS deviation from $3\,\mathrm{dB}$ of the mode-averaged linear NFs expressed in dB, and $\Phi = 1$ ($\Phi \gg 1$) for realizations with gain and NF values inside (outside) the range of interest, in this case, with modal gains between the 10-dB span attenuation and up to $2\,\mathrm{dB}$ greater, and modal NFs over $3\,\mathrm{dB}$. Finally, θ is a weighting parameter tuning the relative priorities of the two terms summed in the objective. We take $\Phi = 1000$, and set θ as a heuristic value between 0 and 1; in the results shown here, $\theta = 1/4$ except for the lowest input signal power per mode of $-5\,\mathrm{dBm}$, where we choose $\theta = 1/2$. We choose bounds for the optimized parameters as: pump spatial mode power less than $300\,\mathrm{mW}$, maximum possible EDF length of $2\,\mathrm{m}$, and doping radii allowed to vary freely within the fiber core and trench. In general, the choice of maximum EDF length will depend on the erbium doping concentration and fiber core diameter. The value of $2\,\mathrm{m}$ is chosen here based on preliminary optimizations, which all converged to solutions with EDF lengths above but close to $1\,\mathrm{m}$, and suitably low pump powers. Optimizations with maximum EDF lengths of $5\,\mathrm{m}$ or $10\,\mathrm{m}$ produced the same solutions.

The PSO algorithm of MATLAB is used with a swarm size of 500, objective function stopping tolerance of 10^{-3}, and at most 10 stall iterations. To speed up computations using the MM-EDFA model within the optimization iterations while ensuring good performance over the C-band, we make two adjustments: first, in the optimization iterations we discount the coupling terms from the amplifier coupled-mode propagation equations, which are typically orders of magnitude lower than the gain coefficients of the modes themselves, and put them back in for the forward evaluation of the performance achieved with the optimized parameters; second, we perform the optimization at only two wavelengths, $1530\,\mathrm{nm}$ and $1565\,\mathrm{nm}$, and after optimization, perform a forward evaluation by running simulations with the optimized parameters for 40 wavelengths, while holding the total power over all signal modes and wavelengths constant. We specify the target values at the two wavelengths to be equal to $(10 + \mu)\,\mathrm{dB}$, where μ is a margin added to the nominal 10-dB span loss at both wavelengths to ensure the gain is not less than the span loss at all wavelengths in between, accounting for variations in the shape of the gain spectrum. In the results shown here, $\mu = 1.25\,\mathrm{dB}$ at both wavelengths, except in the case of the highest input signal power per mode of $5\,\mathrm{dBm}$, where $\mu = 1.75\,\mathrm{dB}$ at $1530\,\mathrm{nm}$. For the procedure outlined here, an optimization run on the Stanford Sherlock HPC cluster using 32 cores with 32 GB RAM in parallel completes within 16 hours.

The choice of μ may be fine-tuned by system designers. For example, higher margins may be added to accommodate different per-span losses, and the target gain may be specified at more than two wavelengths, or over each of the six spatial modes in order to compensate for possible systematic mode-dependent losses in the transmission system.

B. Pump Coupler Design

We design a wavelength- and mode-selective PC to efficiently couple pump light into the fourth mode group at $980\,\mathrm{nm}$ (LP_{12a}, LP_{12b}, LP_{31a}, LP_{31b}), while transmitting the six co-propagating

[1] In strongly coupled long-haul links, the impact of MDG depends on σ_g, which is the STD of the modal gains, each expressed in dB [17], [60], [61], while the impact of ASE can be quantified in terms of 10 times the base-10 logarithm of the mean of the modal NFs, each expressed in W/W [60], [62].

signal modes near 1550 nm. We employ weakly coupled mode-selective couplers (MSCs) [63], which operate by matching the propagation constants of a desired mode in a MMF and the fundamental mode in a closely positioned SMF. MSCs and tapered-velocity MSCs are often used for mode-selective (de)multiplexing of signal modes in the C-band [63], [64], [65], [66], [67]. For our wavelength- and mode-selective PC, the design objectives are somewhat different [68], [69]:

i) high coupling efficiency to the desired pump modes at 980 nm,
ii) minimal power transfer to other pump modes at 980 nm,
iii) minimal loss for the signal modes near 1550 nm, and
iv) coupling lengths not exceeding a few centimeters.

An MSC designed to couple into low-order pump modes at 980 nm would struggle to meet requirements iii) and iv). These low-order modes are strongly confined, and have weak evanescent fields. Coupling to them within a coupling length of centimeters would require positioning the SMF very close to the MMF core, which would cause excessive losses for the signal modes. As a consequence, only MSCs designed to couple into the fourth or fifth pump mode group can meet all the requirements i)–iv).

MSC design is based on coupled-mode theory [70]. Considering a simple case in which there is only one mode in a MMF with non-zero coupling to the SMF, the maximum coupling efficiency of the MSC is given by [63]

$$\eta \approx \frac{1}{1+\left(\frac{\Delta\beta}{2C}\right)^2}, \tag{2}$$

where $\Delta\beta$ is the difference between the modal propagation constants and C is the coupling coefficient between the two modes. The maximum coupling efficiency η approaches 100% when the propagation constants of the two modes are equal. The length at which maximum power transfer occurs is [63]

$$L_C = \frac{\pi\sqrt{\eta}}{2C}. \tag{3}$$

Hence, the larger the coupling coefficient C, the shorter the coupling length L_C.

In our design, only two different MSCs are designed for coupling into either the LP_{12} or LP_{31} modes. Each LP mode LP_{lm}, with non-zero azimuthal number l, contains two orthogonal and degenerate spatial modes LP_{lma} and LP_{lmb} with transverse field profiles $R_{lm}(r)\cos(l\phi)$ or $R_{lm}(r)\sin(l\phi)$, respectively. Therefore, we can independently couple into the a and b modes by positioning two identical SMF cores in series separated by angle $\pi/2\,l + n\pi/l$ for $n = \{0, 1, 2, \ldots\}$ [67]. A $\pi/2$ rotation between these two identical cores, as shown in Fig. 3, enables independent coupling into the a and b modes. It is important to couple mutually incoherent sources into the LP_{lma} and LP_{lmb} so the pump mode fields add incoherently to maintain an axially symmetric pump power distribution. Coherent addition of the pump mode fields would induce a non-axially symmetric pump power distribution that would depend on the phase difference between modes. This would induce unwanted differences in gain between degenerate modes.

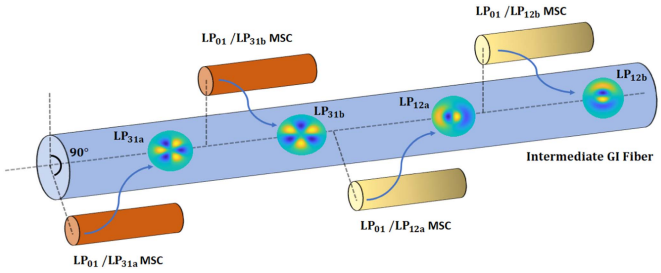

Fig. 3. Proposed wavelength- and mode-selective pump coupler (PC) for coupling four pump modes at 980 nm into an intermediate GI coupling fiber with six co-propagating signal modes near 1550 nm. The PC is composed of two LP_{01}/LP_{31} mode-selective couplers (MSCs, in orange) and two LP_{01}/LP_{12} MSCs (in yellow) in series. Within each pair, the first and second MSCs are angularly separated by 90° to couple independently into the a and b modes, respectively.

TABLE I
MODE-SELECTIVE COUPLER DESIGN PARAMETERS

	r_{core} (μm)	Δ	d (μm)	L_C (cm)
LP_{01}/LP_{12}	1	11.354×10^{-3}	18	5.150
LP_{01}/LP_{31}	1	11.495×10^{-3}	18	3.226

Coupling to the pump modes in the transmission or amplification MMFs, which have the index profile shown in Fig. 2, would be challenging. While trench-assisted GI fibers with $\alpha \approx 2$ are suitable for transmission, these fibers have mode degeneracies that are not conducive to mode-selective coupling. Since the LP_{12} and LP_{31} modes are nearly degenerate in these fibers, an MSC using an SMF phase-matched to the LP_{12} pump mode would also simultaneously couple to the LP_{31} pump mode, causing undesirable coherent addition of pump modes. Moreover, the trench greatly reduces the coupling coefficient by suppressing the evanescent fields of the fiber modes, making the coupling efficiency more sensitive to propagation constant mismatch, and increasing the coupling length. We therefore design an intermediate GI fiber for coupling. The intermediate fiber is a trench-less GI fiber with $\alpha = 1.6$, core relative index difference $\Delta = 0.63\%$, and core radius $r_{\text{core}} = 13$ μm. This value of α breaks the unwanted near-degeneracy between the desired pump modes. The MSCs can now be designed conventionally to use SMF cores phase-matched to the individual pump modes. Splicing from the transmission fiber to the intermediate fiber and back will cause loss, which will be quantified in Section III-B.

The characteristics of the LP_{01}/LP_{12} and LP_{01}/LP_{31} MSCs are given in Table I. The phase-matched SMFs are step-index fibers defined by the core radius r_{core} and relative index difference Δ. The core radius of the phase-matched SMFs is fixed at 1 μm, while the relative index difference is allowed to vary. The distance between cores is $d = 18$ μm for both MSCs. This distance is chosen to ensure a coupling coefficient small enough to maintain minimal power transfer to unwanted LP modes and large enough to achieve a coupling length of the order of centimeters. The performance of the MSC designs will be discussed in Section III-B.

TABLE II
MULTIMODE AMPLIFIER PARAMETERS OPTIMIZED AT TWO WAVELENGTHS

EDFA input signal power per mode (dBm)	EDF length (m)	Doping radius (μm)		Pump mode power (mW)		MDG STD σ_g (dB)		Mode-averaged linear NF (dB)	
		Inner	Outer	$LP_{12a,b}$	$LP_{31a,b}$	1530 nm	1565 nm	1530 nm	1565 nm
−5.0	1.148	1.45	10.69	50.5	21.4	0.25	0.43	5.15	3.74
−2.5	1.116	0.24	11.06	61.3	34.3	0.08	0.25	5.10	3.73
0	1.096	0.00	11.97	93.3	49.3	0.02	0.12	5.05	3.72
2.5	1.084	0.00	14.72	152.0	73.8	0.01	0.04	5.02	3.71
5.0	1.048	0.33	17.20	259.3	136.2	0.22	0.08	4.81	3.64

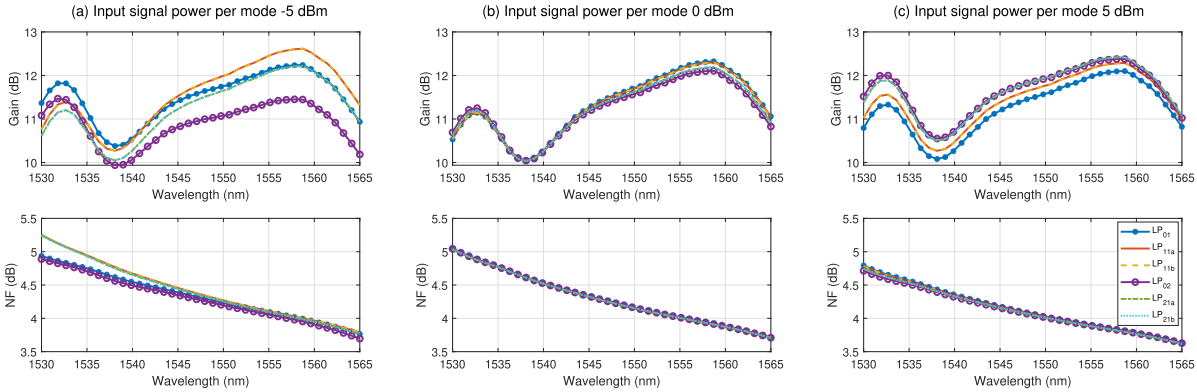

Fig. 4. Modal gains (top row) and NFs (bottom row) vs. wavelength for the optimized MM-EDFs in Table II at input signal powers of (a) −5 dBm, (b) 0 dBm, (c) 5 dBm per mode, or −21, −16, −11 dBm per mode per wavelength, respectively. The legend for the spatial modes in (c) applies to all gain and NF curves.

III. RESULTS

A. Amplifier Performance

Optimizing the amplifier as described in Section II-A at the 1530 and 1565 nm wavelengths over a range of input signal powers, we obtain the MM-EDF parameters shown in the center columns of Table II, along with the resulting minimized MDG STD σ_g and mode-averaged linear NF values shown in the right columns. The lowest MDG values are achieved with input signal powers per spatial mode from 0 to 2.5 dBm. The NFs decrease slightly with increasing input signal power and, as expected, decrease significantly with increasing wavelength. The optimized EDF lengths, which are of the order of just 1 m, as in [27], decrease slightly with increasing input signal power. The optimized ring-doped region expands with increasing input signal power, presumably because at higher powers, inner- and outer-core doping regions may be better inverted. The optimized pump powers increase with increasing input signal power, as expected. At all input signal powers, there is a clear preference for higher power in the LP_{12} pump modes than in the LP_{31} pump modes, presumably because the former overlap more strongly than the latter with the collective signal modes.

Fig. 4 shows the modal gain and NF curves for the amplifiers of Table II obtained by forward simulation over 40 wavelengths in the C-band for the input signal powers per mode of $-5, 0, 5$ dBm, or $-21, -16, -11$ dBm per mode per wavelength, respectively. At all input signal powers, at least 10 dB of gain is provided across the C-band to compensate for the overall span loss (this includes the multimode isolator and GFF+LPFG shown in Fig. 1, which may induce up to 2 dB mode-averaged loss). Forward simulations over 20 wavelengths with 3 dB higher input powers (or 10 wavelengths with 6 dB higher powers) yield similar modal gains and NFs, affirming the sufficiency of simulating 40 wavelengths.

Fig. 5(a) presents the MDG STD σ_g vs. wavelength curves for the optimized MM-EDFs of Table II at the input signal power per mode values shown, as obtained from forward simulation over 40 wavelengths in the C-band. The dot-dashed curves represent the performance of the MM-EDFs alone, while the solid curves also include PC and splice losses, which are evaluated in detail in the following subsection. The trends of optimized MDG with input signal power per mode are similar to those in Table II, with the lowest MDG STD of $\sigma_g < 0.1$ dB over the entire C-band obtained at an input signal power of 2.5 dBm.

Fig. 5(b) presents the corresponding mode-averaged linear NF vs. wavelength curves. The trends of optimized amplifier NFs are again similar to those in Table II, decreasing with increasing input signal power and with increasing wavelength, with a variation over the C-band of 1.15 to 1.4 dB.

Finally, we explore the performance achievable over a range of input signal powers if the MM-EDF design is fixed and only the pump mode powers are optimized. The MM-EDF has 1 m length and full-core doping up to 17.25 μm radius, with 9.96×10^{24} m^{-3} doping concentration. The results, presented in Table III, exhibit trends similar to Table II, with generally higher optimized pump powers, higher MDG STDs, and slightly lower NFs than for the fully optimized MM-EDFs. At the highest input signal powers, 2.5 to 5 dBm, the MDG and NF performance meets or exceeds that for the fully optimized MM-EDFs, although higher pump powers are required. In summary, optimizing all MM-EDF properties (length, doping radii and pump mode powers) is most beneficial in reducing MDG, NF and pump power at low input signal powers.

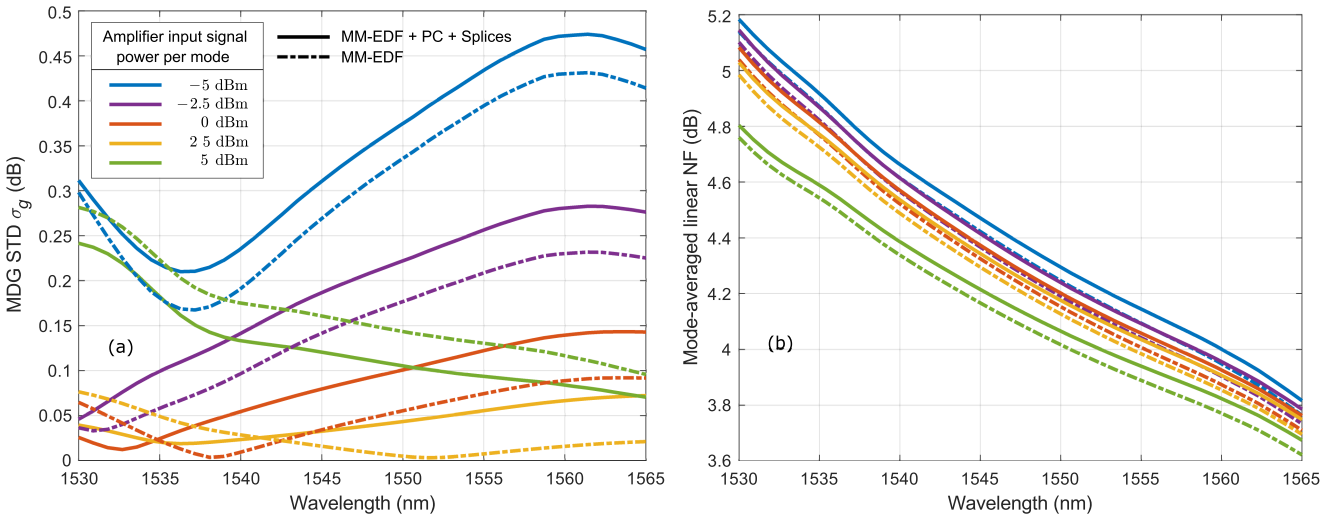

Fig. 5. (a) MDG STD σ_g, and (b) mode-averaged linear NF, vs. wavelength for the optimized MM-EDFs in Table II at the input signal powers per mode indicated. Dot-dashed curves represent results from Section III-A for the MM-EDFs themselves, while solid curves include the PC and splice losses evaluated in Section III-B. The legend in (a) also applies to (b).

TABLE III
MULTIMODE AMPLIFIER PUMP POWERS OPTIMIZED AT TWO WAVELENGTHS FOR 1 m-EDF WITH FULL-CORE DOPING

EDFA input signal power per mode (dBm)	Pump mode power (mW)		MDG STD σ_g (dB)		Mode-averaged linear NF (dB)	
	$LP_{12a,b}$	$LP_{31a,b}$	1530 nm	1565 nm	1530 nm	1565 nm
−5.0	62.8	21.2	0.91	0.43	5.10	3.71
−2.5	67.4	37.3	0.67	0.34	5.06	3.69
0	109.5	46.3	0.27	0.15	4.93	3.65
2.5	160.4	75.8	0.01	0.04	4.87	3.63
5.0	261.7	141.3	0.23	0.07	4.74	3.59

TABLE IV
PUMP MODE COUPLING EFFICIENCIES OF THE PUMP COUPLER

Pump Modes	Pump Coupler		Pump Coupler + Splice	
	LP_{12}	LP_{31}	LP_{12}	LP_{31}
LP_{01}/LP_{12}	99.7%	0.3%	98.6%	1.1%
LP_{01}/LP_{31}	99.3%	0.7%	98.3%	1.5%

B. Pump Coupler Performance

In this subsection, we quantify the pump-mode coupling efficiencies and signal-mode losses of the PC described in Section II-B, including the effect of splices to the transmission and amplification fibers. The constituent MSCs are analyzed using strongly coupled-mode theory [71], which accounts for non-orthogonality of the analyzed modes. Bound and leaky modes are considered to accurately model signal-mode losses. Results of coupled-mode theory are verified using BeamLab [72], a commercial beam propagation software. Splice losses are computed by considering overlaps of mismatched modal fields at the interfaces between the trench-less intermediate coupling fiber and the trench-assisted transmission and amplification fibers [73].

The pump-mode coupling efficiencies of the LP_{01}/LP_{12} and LP_{01}/LP_{31} MSCs are computed using the parameters in Table I. The coupling efficiencies of the PC alone, and including the splice from the coupling fiber to the EDF, are shown in Table IV. The MSCs achieve high coupling efficiencies to the desired pump modes with small power transfer to other modes. Splicing causes only about 0.3% (0.01 dB) loss for both pump modes and weakly couples power between LP_{12} and LP_{31}. Coherent power transfer between pump modes in the PC may affect amplifier performance, but is not studied here.

Signal-mode loss is caused either by splicing to and from the intermediate GI coupling fiber, or by signal-mode coupling into the SMFs of the MSCs or into leaky modes of the intermediate coupling fiber. These loss mechanisms will be referred to as splice loss and coupler loss, respectively. Only coupling to unbound modes contributes to splice loss, since splice-induced coupling between bound LP modes can be compensated by 12×12 multi-input multi-output (MIMO) equalization. Coupler loss is the sum of the signal mode losses from each MSC. Any signal-mode power remaining in the SMF or intermediate GI coupling fiber leaky modes at the end of each MSC is considered lost.

The splice losses and coupler losses for the six signal modes as a function of wavelength are shown in Fig. 6(a) and 6(b), respectively. Splice loss is the more significant loss, inducing the highest losses of 0.09 dB and 0.07 dB loss to the LP_{02} and LP_{21} modes, respectively. These least-bound modes have the largest splice losses because their evanescent fields are most affected by the presence or absence of a trench, causing significant modal

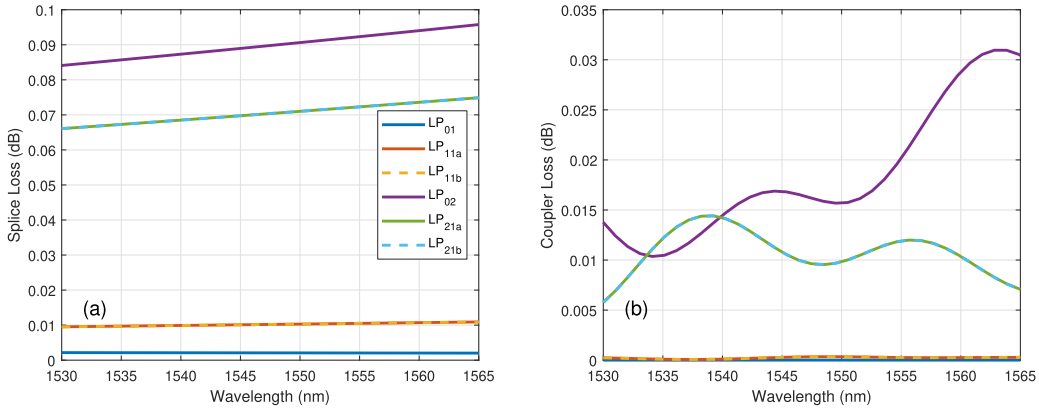

Fig. 6. Signal-mode losses at the PC vs. wavelength over the C-band: (a) splice losses between transmission fiber, intermediate coupling fiber and amplification fiber, and (b) coupler losses from all four MSCs. The legend in (a) also applies to (b).

field mismatches. Coupler loss is less significant, but also has the greatest effect on the least-bound LP_{02} and LP_{21} modes, since their effective indices are closest to the effective index of the LP_{01} mode in the SMF. The effective indices between these signal modes in the intermediate GI coupling fiber and those in the SMFs differ by about 10^{-3} over the C-band, preventing substantial signal loss.

Fig. 5(a) shows how MDL from the coupler and splice losses affects the overall MDG of the amplifier subsystem. At lower input signal powers, the coupler and splice losses *increase* the total amplifier MDG STD σ_g by roughly $0.05\,\mathrm{dB}$ over the C-band; at the best-performing powers of $0\,\mathrm{dBm}$ and $2.5\,\mathrm{dBm}$, there is cross-over between the MDG STD σ_g curves with and without the coupler and splice losses, even as they remain below $0.15\,\mathrm{dB}$; at the highest input signal power, where the ordering of modal gains is reversed and the optimized MM-EDFA provides the most gain to the higher-order LP_{02} and LP_{21} signal modes (see Fig. 4), the coupler and splice losses *decrease* the total amplifier MDG STD σ_g by roughly $0.05\,\mathrm{dB}$.

Fig. 5(b) shows how the coupler and splice losses affect the mode-averaged linear NF of the amplifier subsystem, adding roughly $0.04\,\mathrm{dB}$ across the C-band for all input signal powers.

We consider the effect of possible errors in the angular separation between the two MSCs for the LP_{12} modes or the two MSCs for the LP_{31} modes in the PC. If the two MSCs for each LP-mode pair are not angularly separated by $\pi/2\,l + n\pi/l$ for $n = \{0, 1, 2, \ldots\}$, the second MSC will couple into both the LP_{lma} and the LP_{lmb} modes, instead of just the LP_{lmb} mode. This is shown in Fig. 7. The LP_{31} couplers are much more susceptible to angular offset than the LP_{12} couplers, owing to a higher azimuthal order. Simultaneous coupling into both the LP_{lma} and LP_{lmb} modes will cause unwanted coherent addition of these modes in the amplifier, potentially increasing the MDG. Angular offsets within each MSC pair may be minimized by fabricating the two MSCs separately, cascading them, coupling mutually coherent $980\,\mathrm{nm}$ light into them and adjusting their angular orientations to minimize some signature of coherent addition at the output before fusion splicing them together.

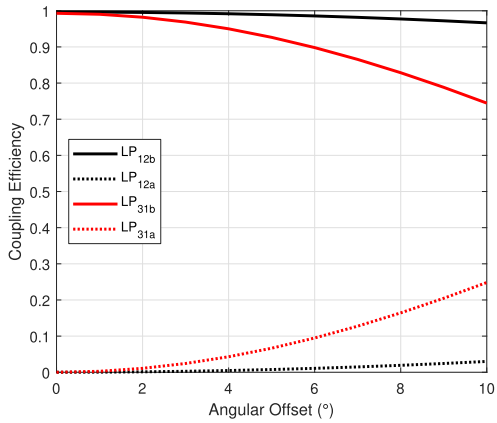

Fig. 7. Coupling efficiencies of the second MSC in Fig. 3 to the LP_{31b} and LP_{31a} modes vs. angular offset from its nominal position, $90°$ from the first MSC (red curves); and coupling efficiencies of the fourth MSC to the LP_{12b} and LP_{12a} modes vs. angular offset from its nominal position, $90°$ from the third MSC (black curves).

An additional performance degradation may arise from refractive index profile errors in the intermediate GI fiber and/or the SMFs that constitute the MSCs. Such errors will cause propagation constant mismatches that reduce pump coupling efficiency. The reduced coupling efficiency can be completely overcome by increasing the pump laser powers, which will decrease system power efficiency but not affect the amplifier gain, NF or MDG.

C. SDM System Design Implications

We now discuss the implications of the proposed amplification scheme for SDM system design in terms of MDG-limited capacity and power efficiency, drawing comparisons to parallel single-mode systems.

1) Impact of MDG on Capacity: As stated above and studied in [17], [74], [75], MDG tolerances for multimode amplifiers in transoceanic ultra-long haul systems are stringent, especially when considering non-ideal receiver architectures such as minimum mean-square error (MMSE)-based equalization. An effective SNR loss is defined here to relate the average capacity

with MDG, $\bar{C}_{\text{mdg}}$, to the ideal capacity without any MDG, C, as [17]

$$\Delta_{\text{mdg}} = 10\ \log_{10}(\text{SNR}) - 10\ \log_{10}(\text{SNR}_{\text{mdg}}), \tag{4}$$

where $\text{SNR} = D\ (2^{C/D} - 1)$ and $\text{SNR}_{\text{mdg}} = D\ (2^{\bar{C}_{\text{mdg}}/D} - 1)$. One can also relate Δ_{mdg} to an equivalent normalized capacity loss $1 - \bar{C}_{\text{mdg}}/C$ [17], [76]. Choosing a maximum tolerable SNR loss or capacity loss determines the maximum allowable per-amplifier MDG STD σ_g for a given link length and starting optical SNR.

We consider links of 50-km MMF spans with $D = 12$ spatial and polarization modes, with our proposed amplifier subsystem placed at the end of each span. We assume strong, random mode coupling from span to span, which may require mode scrambling (see Section IV-C). The tolerable values of MDG STD σ_g, based on average capacities using optimal maximum-likelihood- (ML-) and MMSE-based receivers, are essentially the same as those for the CC-MCF studied in [17] with $D = 14$, and hence we may evaluate the performance of our amplifier subsystem against those requirements. As in [17, Fig. 10(c) and (d)], these estimates assume the most stringent SNR scaling regime under ASE and nonlinear noise accumulation, with an initial optical SNR per mode (SNR/D) of 31 dB, and we consider maximum effective SNR losses Δ_{mdg} of 1 or 2 dB.

Based on the worst-case MDG STD values over the C-band in Fig. 5(a), we observe that the MM-EDFAs optimized for 2.5 dBm input signal power per mode meet these tolerance requirements for all long-haul link lengths given either ML- or MMSE-based receivers, approaching the performance of PDG-limited single-mode EDFA-based systems. MM-EDFAs optimized for 0 dBm input signal power per mode would meet the tolerance requirements for all long-haul link lengths using ML receivers; however, they may suffer up to a 1 dB effective SNR loss in links over 10000 km using MMSE receivers. Likewise, MM-EDFAs optimized for 5 dBm input signal power per mode enable links of up to 4000 km (MMSE receiver-based) and 8000 km (ML receiver-based) with up to 1 dB effective SNR loss, or links of up to 8000 km (MMSE receiver-based) and ML-receiver links of any length with up to 2 dB effective SNR loss. Further sources of MDL in the amplifier subsystem or transmission fiber would shift these findings in favor of MM-EDFAs optimized for higher input signal powers.

2) Power Efficiency: The pump powers per spatial signal mode, $P_p/(D/2) = P_p/6$, considered here are comparable to those in the parallel SMF systems. For the optimized MM-EDFAs of Table II, providing at least 10 dB of gain for amplifier input signal powers per mode of -5, -2.5, 0, 2.5, and 5 dBm, the pump powers per signal mode are about 24, 32, 48, 75, and 132 mW, respectively. Fig. 8 shows, as a function of pump power per spatial mode, the MM-EDFA optical-to-optical PCE

$$\text{PCE} = \frac{P_{s,\text{out}} - P_{s,\text{in}}}{P_p}, \tag{5}$$

where P_p is the total pump power, and $P_{s,\text{in}}$ and $P_{s,\text{out}}$ are the total input and output signal powers respectively, over all wavelengths and modes. In the PCE formula (5), the output signal power is taken directly after the MM-EDF, and does not include the loss of a multimode GFF or dynamic gain equalizer, unlike the single-mode EDFA PCE defined in [1]. The PCEs of the fully optimized MM-EDFAs in Fig. 8 are otherwise similar to those of the single-mode EDFAs with equal pump power per signal spatial mode, being roughly equal near 17 dBm, while being a few percent lower at low pump powers and a few percent higher at high pump powers than the single-mode PCEs. For the amplifiers with fixed 1 m EDF length and full-core doping, and only pump mode powers optimized, the PCEs are roughly 2 to 4% lower than for the fully optimized MM-EDFAs. The gap widens at low pump powers, illustrating the power efficiency advantages of fully optimized MM-EDFAs at lower powers.

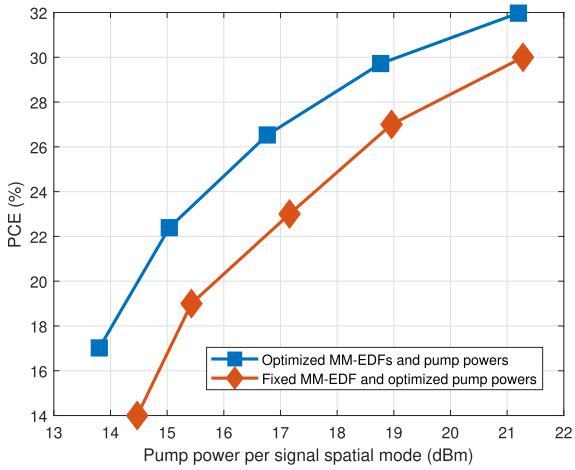

Fig. 8. Amplifier optical-to-optical power-conversion efficiencies (PCEs) with pump power per signal spatial mode ($P_p/6$), for the MM-EDFAs with optimized length, doping radii and pump powers in Table II (blue squares), and those for the MM-EDFAs with fixed length of 1 m, full doping up to 17.25 μm, and optimized pump powers only in Table III (red diamonds).

Pump farming is a strategy of combining the outputs of two or more pump laser diodes in a manifold of 3 dB couplers to enhance the reliability of pumping a fiber pair [58]. The pump manifold for the proposed amplifier subsystem would differ from that in parallel single-mode SDM systems. Since each fiber pair requires eight pump laser diodes (four per fiber), the number of laser diodes and couplers is quadrupled; however, the number of laser diodes and couplers per spatial mode is reduced by a third compared to parallel single-mode systems.

The resulting number of fiber pairs may be estimated using the same formulae as in [1], [77] with a total pump power over all modes P_p, and compared to single-mode system performance, could provide roughly six times the capacity with the same fiber pair count, or equivalently, the same capacity using one sixth of the fiber pair count. This finding assumes overall power efficiencies equivalent to those in parallel SMF SDM experiments [1], [59].

IV. Discussion

In this section, we first discuss how the proposed graded-index MM-EDFs could be manufactured. We then explore how the proposed approach may be extended to MMFs supporting more than six spatial modes, or to CC-MCFs. Finally, we discuss

key challenges for MMF-based long-haul systems—obtaining strong mode coupling and minimizing GD spread—and how these may be addressed.

A. Manufacturing Methods

It would be challenging to manufacture the proposed GI MM-EDFs using current commercial fabrication techniques, which employ modified chemical vapor deposition (MCVD) with solution doping of the erbium and co-dopants [78]. This process is limited by fiber geometry and homogeneity issues [79], and is best suited to confined doping in step refractive index profiles. Fortunately, recent developments in MCVD with gas-phase doping show significant promise in overcoming current fabrication limitations. This method has been used to fabricate EDFs with independently defined, piece-wise constant refractive index and erbium doping profiles [80]. Moreover, the vapor-phase chelate delivery technique [81], [82] has demonstrated the capability to realize rare-earth doping in graded refractive index silica fibers [83], and full-core step and ring doping of rare-earth ions in step-index silica fibers [84]. Most recently, gas-phase atomic layer deposition of erbium nanofilms incorporating PbS as a co-dopant has enabled improved control of the concentration and uniformity of the Er^{3+} ions, while yielding beneficial amplifier properties of large gain bandwidth and low NF [85]. Further extensions and refinements of such manufacturing techniques to improve their flexibility, uniformity and repeatability should enable fabrication of the proposed GI MM-EDFs with ring erbium doping.

B. Integration and Scaling

Integration is a key to scaling SDM systems beyond parallel SMFs [76]. We have demonstrated amplification of six signal spatial modes while exciting only the fourth pump mode group, which comprises only four of the 15 available pump spatial modes. Notably, we choose higher-order pump modes, LP_{12} and LP_{31}, because MSCs can efficiently couple the pump to them while inducing low signal-mode loss. This approach might be extended to amplify 10 signal spatial modes by designing MSCs to excite the fifth or sixth pump mode groups. By contrast, designing MSCs with low signal-mode loss for coupling into low-order pump modes, such as LP_{01} or LP_{11}, becomes progressively more difficult for an increasing number of signal modes.

CC-MCFs have demonstrated superior long-haul transmission properties [16], including large modal effective areas to minimize nonlinearity, and distributed strong mode coupling to minimize accumulation of GD and MDL/MDG. Multicore amplification, however, typically employs complicated, lossy fan-out/fan-in with single-mode amplifiers or inefficient, cladding-based pumping of multicore amplifiers [20], [21], [22], [23], [24], [25], [26], [27], [28]. The wavelength- and mode-selective pumping scheme proposed here may perhaps be extended to efficiently pump multicore amplifiers, provided all the cores are accessible from the fiber periphery. The number of coupling fibers would need to equal the number of cores, assuming there is negligible pump coupling between cores. This would not achieve the advantage demonstrated here with multimode amplifiers, where the number of pump spatial modes is smaller than the number of signal spatial modes amplified. For strong coupling between cores at the pump wavelength also [86], there may be added challenges controlling core-dependent saturation and pump propagation in the common cladding.

C. Mode Coupling and Modal Dispersion

Achieving strong mode coupling and reducing modal dispersion are the main challenges facing MMF transmission systems. CC-MCFs offer strong mixing between all modes over short coupling lengths [8], [14], so GD spreads accumulate with the square root of fiber length rather than linearly. The challenge of large GD spreads persists in MMFs, which have significant effective index differences between mode groups, so random perturbation-induced inter-group coupling is weak, although intra-group coupling is strong. Designing MMF refractive index profiles for strong inter- *and* intra-group coupling, while maintaining low guided-mode and high leaky-mode losses, is an outstanding challenge that may not be practically surmountable [87]. Larger GD spreads result in higher digital signal processing (DSP) complexity and longer adaptation times at the receiver. MMF systems may thus offer the advantage of integration in the wet plant amplifier subsystem at the expense of the dry plant receiver DSP complexity, a trade-off counter to CC-MCF-based systems, which offer the advantage of strong, random coupling among all modes, but pose challenges in integrating amplification.

In MMF systems, strong, random mode coupling can be achieved by placing an LPFG or other type of mode scrambler in each span. Per-span mode scrambling, corresponding to a coupling length equal to the span length, is sufficient to minimize the accumulation of amplifier MDG [88], [89] and helps reduce the accumulation of GD spread with link distance. The GD reduction may be insufficient in transoceanic systems, so receiver-side DSP complexity may be high [90], with filters requiring several hundred taps to compensate for modal dispersion. Among options for mode scramblers, LPFGs offer the advantage of high integration, and may be placed in-line with the isolator and gain-flattening components in each span [91]. To date, LPFGs have mode-averaged losses less than $0.45\,\mathrm{dB}$ and MDL STDs less than $0.36\,\mathrm{dB}$ over the C-band [88], [92]. These losses, especially the MDL, must be reduced several-fold to satisfy the requirements for transoceanic systems (see Section III-C1). This reduction may perhaps be achieved by a novel design strategy that suppresses coupling between guided and leaky modes.

GD compensation holds promise for counteracting the larger accumulated GD spreads in MMF, thereby reducing receiver DSP complexity [93], [94]. This strategy involves designing fibers with opposing modal GD orderings, which are concatenated within each link span. Here, we propose to modify the transmission fiber index profile shown in Fig. 2, while keeping within the same maximum F doping concentration and guided-mode loss constraints. We consider two-fiber and three-fiber GD-compensating designs. Following the approach of [95], we consider trench-assisted GI fibers parameterized by six parameters: r_{core} is the core radius, Δ is the relative index difference of

TABLE V
MULTI-FIBER COMPENSATION SCHEMES

	r_{core} (μm)	Δ	α	w_{gap} (μm)	Δ_{trench}	w_{trench} (μm)	R
Two-Fiber	12.70	6.00×10^{-3}	1.8137	0.46	1.4505×10^{-3}	6.80	1.00
	13.00	6.00×10^{-3}	2.0372	0.00	1.4600×10^{-3}	6.66	2.00
Three-Fiber	12.70	5.99×10^{-3}	1.8500	0.52	1.4362×10^{-3}	6.30	1.00
	13.00	6.00×10^{-3}	2.0000	0.00	1.4600×10^{-3}	6.99	2.89
	13.00	6.00×10^{-3}	1.9002	0.20	1.4589×10^{-3}	6.64	0.33

the core, α is the GI exponent, w_{gap} is the radial distance between the end of the GI core and the beginning of the trench, w_{trench} is the width of the trench, and Δ_{trench} is the relative index difference of the trench. We use a PSO algorithm to optimize all the fiber parameters for the two-fiber and three-fiber compensating schemes. In the presence of intergroup and intragroup mode coupling, it is beneficial to have shorter segments of the two or three compensating fibers cyclically repeated M times within a span [93], [94]. The span length of a system with M repeating n-fiber segments is given by $L_{\text{span}} = M \sum_{i=1}^{n} L_i$, where L_i is the length of the ith fiber in each segment. The ratios of fiber lengths relative to the first, $R_j = L_j/L_1$, are determined by a convex optimization that minimizes a weighted sum of the GD STDs after propagation through each fiber segment at select wavelengths, chosen here to be $1530\,\text{nm}$, $1550\,\text{nm}$, and $1565\,\text{nm}$.

For a general n-fiber optimization scheme, in which the ith fiber supports $D/2$ spatial modes at wavelength λ_k with uncoupled zero-mean GDs $\boldsymbol{\tau}_i^{\lambda_k} = (\tau_{i,1}^{\lambda_k}, \tau_{i,2}^{\lambda_k}, \ldots, \tau_{i,D/2}^{\lambda_k})$, the optimal length ratios, R_i, can be determined by the following convex problem:

$$\text{minimize} \ \frac{1}{\sqrt{D/2}} \sum_{k} \left\| \boldsymbol{\tau}_1^{\lambda_k} + \sum_{i=2}^{n} R_i \boldsymbol{\tau}_i^{\lambda_k} \right\| \tag{6}$$

$$\text{subject to} \ R_i \leq R_{\text{upper}} \tag{7}$$

$$R_i \geq R_{\text{lower}}, \tag{8}$$

where i indexes the fiber, and k indexes the wavelength. The minimized sum in (6) is then normalized by the sum of the length ratios to obtain the equivalent modal dispersion summed over selected wavelengths. Ideally, division by the sum of the length ratios should be included within the objective (6); including it, however, would render the minimization non-convex. This compromise for convexity nevertheless yields reasonable solutions, which are found using the CVX software package [96], [97]. PSO is then applied to obtain the optimal fiber parameters minimizing the objective (6), subject to bounds on the length ratios, R_{upper} and R_{lower}, which are set to ensure the fiber lengths are non-trivial.

Additional constraints are imposed on the parameter space to ensure six spatial modes for each fiber, to keep refractive index profiles within F-doping limits, and to comply with leaky- and guided-mode bending loss standards [52], [53], all of which the original transmission fiber in Fig. 2 satisfies. The most significant restrictions on the parameter space result from the leaky-mode bending loss standard. Small variations in the core radius, core relative index difference, α exponent, and gap width parameter values impact leaky-mode bending losses. To simplify the parameter-space restrictions while preventing deleterious multipath transmission interference or amplification of unwanted modes due to leaky-mode propagation, only one fiber in each of the two- and three-fiber schemes is constrained to satisfy the leaky-mode loss requirement. All fibers satisfy the guided-mode bending loss requirement.

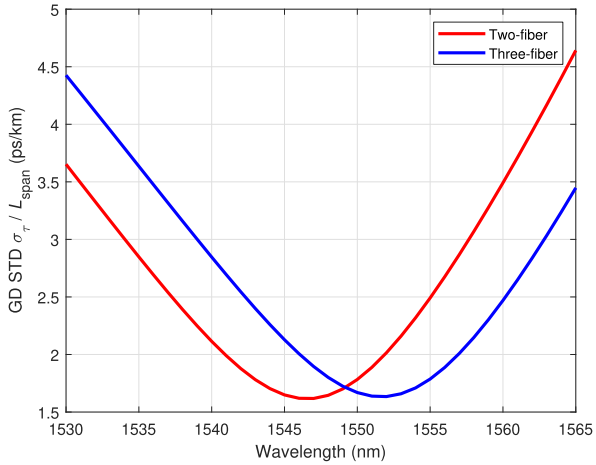

Fig. 9. Equivalent GD STDs of two-fiber (red) and three-fiber (blue) compensating schemes as a function of wavelength over the C-band. The optimized fiber parameters for the schemes are given in Table V.

The optimized fiber parameters and fiber length ratios, R, for two-fiber and three-fiber GD compensation schemes are given in Table V. The equivalent GD STDs $\sigma_\tau/L_{\text{span}}$ of both designs over the C-band are shown in Fig. 9. For both designs, we obtain minimum $\sigma_\tau/L_{\text{span}} \approx 1.6\,\text{ps/km}$ near $1550\,\text{nm}$ and maximum $\sigma_\tau/L_{\text{span}} \approx 4.5\,\text{ps/km}$ at either 1530 or $1565\,\text{nm}$. Going from the two-fiber to the three-fiber design decreases the optimization objective (6) and the maximum $\sigma_\tau/L_{\text{span}}$ by only about 5%, likely because of the imposed parameter-space restrictions. We observe that in both schemes, the optimal fiber parameters of all but the first spans assume the upper bounds of the core radius, $13\,\mu\text{m}$, and of the core relative index difference, 6.0×10^{-3}. The mode-averaged chromatic dispersions of all fibers in both designs range from 19 to $23\,\text{ps/nm/km}$ over the C-band, like the original fiber shown in Fig. 2.

Considering the three-fiber compensation scheme (blue curve in Fig. 9), at the worst-case wavelength of $1530\,\text{nm}$, the GD STD after a $50\,\text{km}$ span is $\sigma_\tau = 225\,\text{ps}$. With strong, random coupling induced by a mode-scrambling LPFG in each span, the required number of receiver equalizer taps at the end of a link of K spans is given by [98]

$$N_{\text{md}} = \lceil \sigma_{\text{gd}} \, u_D(p) \, r_{\text{os}} \, R_{\text{s}} \rceil, \tag{9}$$

where $\sigma_{\text{gd}} = \sigma_\tau \sqrt{K}$, $u_D(p) \approx 4.6$ for $D = 12$ with probability $1 - p = 1 - 10^{-6}$ [98], [99], r_{os} is the oversampling ratio and R_{s} the symbol rate. For example, a $10000\,\text{km}$ link of $K = 200$ spans at $R_{\text{s}} = 48\,\text{GBaud}$ with $r_{\text{os}} = 16/15$ (see, e.g., [100]) would require $N_{\text{md}} \approx 750$ taps. At the best-case wavelength for three-fiber compensation near $1552\,\text{nm}$, the required number of filter taps would be about three times smaller. N_{md} is thus predicted to be between 6 to 18 times lower than N_{cd}, the number of taps required for chromatic dispersion compensation at the same link distance.

Assuming adaptive 12×12 MIMO frequency-domain equalization using a cyclic prefix (CP) of length N_{md} at the receiver [101], implementing the discrete Fourier transforms by fast Fourier transforms (FFTs) with block length $N_{\text{fft}} = 2^{12}$ would achieve a CP efficiency $N_{\text{fft}}/(N_{\text{fft}} + N_{\text{md}})$ of 84.5%. The least-mean-squares (LMS) and recursive least-squares (RLS) algorithms were found in [101] to adapt similar 12×12 MIMO equalizers using 700 and 350 training blocks, respectively. For the design parameters considered here, these correspond to adaptation times of about 66 μs and 33 μs for LMS and RLS, respectively. Further study using dynamic channel models [102] calibrated by experimental measurements in deployed fibers may more definitively address the adaptation and tracking behavior of these adaptive MIMO equalizers. Nevertheless, it is desirable to reduce the end-to-end GD spread and the corresponding value of N_{md} in order to ensure fast adaptation and tracking while maximizing CP efficiency and minimizing receiver DSP complexity.

Future work to address the challenges of MMF transmission should target improvements in the two directions outlined here: enhancing mode coupling through novel designs of fibers or mode scramblers, and reducing GD spreads via improved compensation schemes.

V. Conclusion

We have proposed an integrated multimode amplification subsystem based on optimized design of a MM-EDFA and a wavelength- and mode-selective PC. By optimizing the length and ring doping profile of the MM-EDF and optimizing the pump-mode powers, we are able to obtain low MDG, low NF and high PCE. Likewise, by judiciously choosing the pump mode group and the index exponent of an intermediate GI coupling fiber, we are able to design a pump coupler with high pump-mode efficiency and low signal-mode loss. The proposed design uses fewer pump laser diodes per signal than parallel SMF-based systems, and may provide a path for economical, efficient scaling of SDM long-haul systems.

Appendix A
Optimization Objective

The optimization objective (1) may be directly related to, and is one that maximizes, the capacity of a multimode system. We begin by writing an MDG-limited capacity metric

$$C = D\,\log_2\left(1 + \frac{\text{SNR}}{D}\,10^{-\Delta_{\text{mdg}}/10}\right), \tag{10}$$

where Δ_{mdg} is the effective SNR loss in dB caused by MDG [17]. Assuming a signal power P_s per mode and noise power after K amplifiers given by $Kh\nu\,\Delta\nu$ NF, where h is Planck's constant, ν is the channel frequency within the C-band, $\Delta\nu$ is the channel bandwidth, and NF is the mode-averaged linear noise figure [60], the capacity metric becomes

$$C = D\,\log_2\left(1 + \frac{P_s}{Kh\nu\,\Delta\nu}\,\frac{10^{-\Delta_{\text{mdg}}/10}}{\text{NF}}\right). \tag{11}$$

The logarithm is one-to-one and monotonically increasing, so ignoring positive constants, maximizing capacity amounts to minimizing the sum of the effective SNR loss due to MDG and the amplifier NF expressed in dB, i.e., $\Delta_{\text{mdg}} + \text{NF}\,(\text{dB})$.

For moderate-to-large MDG of $\sigma_{\text{mdg}} \geq 3\,\text{dB}$, Δ_{mdg} scales roughly linearly with the MDG STD σ_{mdg} expressed in dB, with the constant of proportionality ranging from $\sim 1/2$ at low SNR of 5 dB to ~ 1 at high SNR of 20 dB [17, Fig. 2]. For a large number of spans, $K \gg 1$, assuming the link is in the strongly coupled regime with overall MDG $\xi = \sqrt{K}\,\sigma_g$,

$$\sigma_{\text{mdg}} = \xi\sqrt{1 + \frac{\xi^2}{12}} \approx \frac{K\,\sigma_g^2}{\sqrt{12}}. \tag{12}$$

Hence, maximizing capacity is equivalent to minimizing the sum of the amplifier MDG STD σ_g and the mode-averaged linear NF, both expressed in dB. The specific form of the objective function used in this work reflects this principle, in addition to that of favoring desired values for gain and NF based on the link parameters, particularly the span attenuation.

The optimization capacity metric could include a dependence on the total optical bandwidth used, which we have dropped, assuming it to be fixed, corresponding to the C-band. Finally, for feed-power-limited MMF systems, the capacity metric may be altered to explicitly maximize the power efficiency, C/P_p, as was done for parallel SMF systems [1]. Inclusion of a term controlling the pump power in the objective function was not found to significantly influence the optimized amplifier designs presented here.

Acknowledgment

Much of the computing for this project was performed on the Sherlock cluster at Stanford University. We thank the Stanford Research Computing Center for providing this cluster and technical support.

References

[1] H. Srinivas et al., "Modeling and experimental measurement of power efficiency for power-limited SDM submarine transmission systems," *J. Lightw. Technol.*, vol. 39, no. 8, pp. 2376–2386, Apr. 2021.
[2] O. V. Sinkin, A. V. Turukhin, W. W. Patterson, M. A. Bolshtyansky, D. G. Foursa, and A. N. Pilipetskii, "Maximum optical power efficiency in SDM-based optical communication systems," *IEEE Photon. Technol. Lett.*, vol. 29, no. 13, pp. 1075–1077, Jul. 2017.
[3] O. V. Sinkin et al., "SDM for power-efficient undersea transmission," *J. Lightw. Technol.*, vol. 36, no. 2, pp. 361–371, Jan. 2018.
[4] J.-X. Cai et al., "9 Tb/s transmission using 29 mW optical pump power per EDFA with 1.24 Tb/s/W optical power efficiency over 15,050 km," *J. Lightw. Technol.*, vol. 40, no. 6, pp. 1650–1657, Mar. 2022.

[5] W. Klaus et al., "Advanced space division multiplexing technologies for optical networks [invited]," *J. Opt. Commun. Netw.*, vol. 9, no. 4, pp. C1–C11, 2017.

[6] P. Sillard, "Few-mode fibers for space division multiplexing," in *Proc. Opt. Fiber Commun. Conf.*, 2016, pp. 1–53. [Online]. Available: http://opg.optica.org/abstract.cfm?URI=OFC-2016-Th1J.1

[7] T. Hasegawa, Y. Yamamoto, and M. Hirano, "Optimal fiber design for large capacity long haul coherent transmission," *Opt. Exp.*, vol. 25, no. 2, pp. 706–712, Jan. 2017. [Online]. Available: http://opg.optica.org/oe/abstract.cfm?URI=oe-25-2-706

[8] M.-J. Li and T. Hayashi, "Chapter 1 - Advances in low-loss, large-area, and multicore fibers," in *Opt. Fiber Telecommun. VII*, A. E. Willner, Ed. San Diego, CA, USA: Academic, 2020, pp. 3–50. [Online]. Available: https://www.sciencedirect.com/science/article/pii/B9780128165027000014

[9] Y. Tamura et al., "The first 0.14-dB/km loss optical fiber and its impact on submarine transmission," *J. Lightw. Technol.*, vol. 36, no. 1, pp. 44–49, Jan. 2018.

[10] V. Sleiffer et al., "A comparison between SSMF and large-A(ef)f pure-silica core fiber for ultra long-haul 100 G transmission," *Opt. Exp.*, vol. 19, no. 26, pp. B710–B715, Dec. 2011. [Online]. Available: http://opg.optica.org/oe/abstract.cfm?URI=oe-19-26-B710

[11] A. Carena, V. Curri, G. Bosco, P. Poggiolini, and F. Forghieri, "Modeling of the impact of nonlinear propagation effects in uncompensated optical coherent transmission links," *J. Lightw. Technol.*, vol. 30, no. 10, pp. 1524–1539, May 2012.

[12] C. Antonelli, O. Golani, M. Shtaif, and A. Mecozzi, "Nonlinear interference noise in space-division multiplexed transmission through optical fibers," *Opt. Exp.*, vol. 25, no. 12, pp. 13055–13078, Jun. 2017. [Online]. Available: http://opg.optica.org/oe/abstract.cfm?URI=oe-25-12-13055

[13] S. O. Arik and J. M. Kahn, "Coupled-core multi-core fibers for spatial multiplexing," *IEEE Photon. Technol. Lett.*, vol. 25, no. 21, pp. 2054–2057, Nov. 2013.

[14] T. Hayashi, Y. Tamura, T. Hasegawa, and T. Taru, "Record-low spatial mode dispersion and ultra-low loss coupled multi-core fiber for ultra-long-haul transmission," *J. Lightw. Technol.*, vol. 35, no. 3, pp. 450–457, Feb. 2017. [Online]. Available: http://opg.optica.org/jlt/abstract.cfm?URI=jlt-35-3-450

[15] Y. Su, Y. He, H. Chen, X. Li, and G. Li, "Perspective on mode-division multiplexing," *Appl. Phys. Lett.*, vol. 118, no. 202021, Art. no. 200502, doi: 10.1063/5.0046071.

[16] G. Rademacher et al., "A comparative study of few-mode fiber and coupled-core multi-core fiber transmission," *J. Lightw. Technol.*, vol. 40, no. 6, pp. 1590–1596, Mar. 2022.

[17] D. A. A. Mello, H. Srinivas, K. Choutagunta, and J. M. Kahn, "Impact of polarization- and mode-dependent gain on the capacity of ultra-long-haul systems," *J. Lightw. Technol.*, vol. 38, no. 2, pp. 303–318, Jan. 2020.

[18] S. Desbruslais, "Maximizing the capacity of ultra-long haul submarine systems," in *Proc. 20th Eur. Conf. Netw. Opt. Commun.*, 2015, pp. 1–6.

[19] Y. Jung, S. ul Alam, D. J. Richardson, S. Ramachandran, and K. S. Abedin, "Chapter 7 - Multicore and multimode optical amplifiers for space division multiplexing," in *Opt. Fiber Telecommun. VII*, A. E. Willner, Ed. San Diego, CA, USA: Academic, 2020, pp. 301–333. [Online]. Available: https://www.sciencedirect.com/science/article/pii/B9780128165027000087

[20] K. S. Abedin et al., "Amplification and noise properties of an erbium-doped multicore fiber amplifier," *Opt. Exp.*, vol. 19, no. 17, pp. 16715–16721, Aug. 2011. [Online]. Available: http://opg.optica.org/oe/abstract.cfm?URI=oe-19-17-16715

[21] K. S. Abedin et al., "Cladding-pumped erbium-doped multicore fiber amplifier," *Opt. Exp.*, vol. 20, no. 18, pp. 20191–20200, Aug. 2012. [Online]. Available: http://opg.optica.org/oe/abstract.cfm?URI=oe-20-18-20191

[22] K. S. Abedin et al., "Multicore erbium doped fiber amplifiers for space division multiplexing systems," *J. Lightw. Technol.*, vol. 32, no. 16, pp. 2800–2808, Aug. 2014.

[23] K. S. Abedin, M. F. Yan, T. F. Taunay, B. Zhu, E. M. Monberg, and D. J. DiGiovanni, "State-of-the-Art multicore fiber amplifiers for space division multiplexing," *Opt. Fiber Technol.*, vol. 35, pp. 64–71, 2017. [Online]. Available: https://www.sciencedirect.com/science/article/pii/S1068520016301079

[24] J. Sakaguchi et al., "19-core MCF transmission system using EDFA with shared core pumping coupled via free-space optics," *Opt. Exp.*, vol. 22, no. 1, pp. 90–95, Jan. 2014. [Online]. Available: http://opg.optica.org/oe/abstract.cfm?URI=oe-22-1-90

[25] Q. Kang, E.-L. Lim, F. Poletti, Y. Jung, S. ul Alam, and D. J. Richardson, "Minimizing differential modal gain in cladding pumped MM-EDFAs for mode division multiplexing in C and L bands," in *Proc. Int. Photon. OptoElectron. Meetings*, 2014, Paper FTh4F.1. [Online]. Available: http://opg.optica.org/abstract.cfm?URI=FBTA-2014-FTh4F.1

[26] C. Jin, B. Ung, Y. Messaddeq, and S. LaRochelle, "Annular-cladding erbium doped multicore fiber for SDM amplification," *Opt. Exp.*, vol. 23, no. 23, pp. 29647–29659, Nov. 2015. [Online]. Available: http://opg.optica.org/oe/abstract.cfm?URI=oe-23-23-29647

[27] Z. S. Eznaveh et al., "Ultra-low DMG multimode EDFA," in *Proc. Opt. Fiber Commun. Conf. Exhib.*, 2017, pp. 1–3.

[28] C. Castro et al., "15 × 200 Gbit/s 16-QAM SDM transmission over an integrated 7-core cladding-pumped repeatered multicore link in a recirculating loop," *J. Lightw. Technol.*, vol. 36, no. 2, pp. 349–354, Jan. 2018.

[29] Y. Yung et al., "First demonstration of multimode amplifier for spatial division multiplexed transmission systems," in *Proc. 37th Eur. Conf. Expo. Opt. Commun.*, 2011, Paper Th.13.K.4. [Online]. Available: http://opg.optica.org/abstract.cfm?URI=ECOC-2011-Th.13.K.4

[30] N. Bai et al., "Mode-division multiplexed transmission with inline few-mode fiber amplifier," *Opt. Exp.*, vol. 20, no. 3, pp. 2668–2680, Jan. 2012. [Online]. Available: https://opg.optica.org/oe/abstract.cfm?URI=oe-20-3-2668

[31] G. Le Cocq, Y. Quiquempois, and L. Bigot, "Optimization algorithm applied to the design of few-mode erbium doped fiber amplifier for modal and spectral gain equalization," *J. Lightw. Technol.*, vol. 33, no. 1, pp. 100–108, Jan. 2015.

[32] S. Jeurink and P. M. Krummrich, "Multimode EDFA designs with reduced MDG by considering spatially dependent saturation effects," in *Proc. Opt. Fiber Commun. Conf.*, 2018, Paper W2A.5. [Online]. Available: http://opg.optica.org/abstract.cfm?URI=OFC-2018-W2A.5

[33] J. Ma, F. Xia, S. Chen, S. Li, and J. Wang, "Amplification of 18 OAM modes in a ring-core erbium-doped fiber with low differential modal gain," *Opt. Exp.*, vol. 27, no. 26, pp. 38087–38097, Dec. 2019. [Online]. Available: http://opg.optica.org/oe/abstract.cfm?URI=oe-27-26-38087

[34] E. Ip et al., "Experimental characterization of a ring-profile few-mode erbium-doped fiber amplifier enabling gain equalization," in *Proc. Opt. Fiber Commun. Conf. Expo. Nat. Fiber Optic Engineers Conf.*, 2013, pp. 1–3.

[35] N. K. Fontaine et al., "Multi-mode optical fiber amplifier supporting over 10 spatial modes," in *Proc. Opt. Fiber Commun. Conf. Exhib.*, 2016, pp. 1–3.

[36] E. Ip, "Gain equalization for few-mode fiber amplifiers beyond two propagating mode groups," *IEEE Photon. Technol. Lett.*, vol. 24, no. 21, pp. 1933–1936, Nov. 2012.

[37] Q. Kang et al., "Accurate modal gain control in a multimode erbium doped fiber amplifier incorporating ring doping and a simple LP01 pump configuration," *Opt. Exp.*, vol. 20, no. 19, pp. 20835–20843, Sep. 2012. [Online]. Available: http://opg.optica.org/oe/abstract.cfm?URI=oe-20-19-20835

[38] X. Huang et al., "Optimized few-mode EDFA of applicability for variable mode groups with an extended doping region and a PSO algorithm," *J. Opt. Soc. Amer. B*, vol. 39, no. 10, pp. 2618–2624, Oct. 2022. [Online]. Available: https://opg.optica.org/josab/abstract.cfm?URI=josab-39-10-2618

[39] N. Bai, E. Ip, T. Wang, and G. Li, "Multimode fiber amplifier with tunable modal gain using a reconfigurable multimode pump," *Opt. Exp.*, vol. 19, no. 17, pp. 16601–16611, Aug. 2011. [Online]. Available: http://opg.optica.org/oe/abstract.cfm?URI=oe-19-17-16601

[40] R. N. Mahalati, D. Askarov, and J. M. Kahn, "Adaptive modal gain equalization techniques in multi-mode erbium-doped fiber amplifiers," *J. Lightw. Technol.*, vol. 32, no. 11, pp. 2133–2143, Jun. 2014.

[41] S. Jeurink and P. M. Krummrich, "Multimode EDFA with scalable mode selective gain control at 1480-nm pump wavelength," *IEEE Photon. Technol. Lett.*, vol. 30, no. 9, pp. 849–852, May 2018.

[42] R. Olshansky, "Mode coupling effects in graded-index optical fibers," *Appl. Opt.*, vol. 14, no. 4, pp. 935–945, Apr. 1975. [Online]. Available: http://opg.optica.org/ao/abstract.cfm?URI=ao-14-4-935

[43] R. Olshansky, "Distortion losses in cabled optical fibers," *Appl. Opt.*, vol. 14, no. 1, pp. 20–21, Jan. 1975. [Online]. Available: http://opg.optica.org/ao/abstract.cfm?URI=ao-14-1-20

[44] P. Sillard, S. Richard, L.-A. de Montmorillon, and M. Bigot-Astruc, "Micro-bend losses of trench-assisted single-mode fibers," in *Proc. 36th Eur. Conf. Exhib. Opt. Commun.*, 2010, pp. 1–3.

[45] X. Jin and F. P. Payne, "Numerical investigation of microbending loss in optical fibres," *J. Lightw. Technol.*, vol. 34, no. 4, pp. 1247–1253, Feb. 2016. [Online]. Available: http://opg.optica.org/jlt/abstract.cfm?URI=jlt-34-4-1247

[46] X. Zheng et al., "Bending losses of trench-assisted few-mode optical fibers," *Appl. Opt.*, vol. 55, no. 10, pp. 2639–2648, Apr. 2016. [Online]. Available: http://opg.optica.org/ao/abstract.cfm?URI=ao-55-10-2639

[47] J. W. Fleming and D. L. Wood, "Refractive index dispersion and related properties in fluorine doped silica," *Appl. Opt.*, vol. 22, no. 19, pp. 3102–3104, Oct. 1983. [Online]. Available: http://opg.optica.org/ao/abstract.cfm?URI=ao-22-19-3102

[48] Y. Chigusa et al., "Low-loss pure-silica-core fibers and their possible impact on transmission systems," *J. Lightw. Technol.*, vol. 23, no. 11, pp. 3541–3550, Nov. 2005.

[49] H. Kakiuchida, N. Shimodaira, E. H. Sekiya, K. Saito, and A. J. Ikushima, "Refractive index and density in F- and Cl-doped silica glasses," *Appl. Phys. Lett.*, vol. 86, no. 16, 2005, Art. no. 161907, doi: 10.1063/1.1897062.

[50] Y. Liu, Z. Yang, J. Zhao, L. Zhang, Z. Li, and G. Li, "Intrinsic loss of few-mode fibers," *Opt. Exp.*, vol. 26, no. 2, pp. 2107–2116, Jan. 2018.

[51] S. Urata, N. Nakamura, K. Aiba, T. Tada, and H. Hosono, "How fluorine minimizes density fluctuations of silica glass: Molecular dynamics study with machine-learning assisted force-matching potential," *Mater. Des.*, vol. 197, 2021, Art. no. 109210. [Online]. Available: https://www.sciencedirect.com/science/article/pii/S0264127520307450

[52] Transmission Media and Optical Systems Characteristics–Optical Fibre Cables Characteristics of a Fibre and Cable With Non-Zero Dispersion for Wideband Optical Transport, Standard ITU-T G.656, ITU, Geneva, Switzerland, 2010.

[53] Optical Fibres–Part 1-44: Measurement Methods and Test Procedures – Cut-Off Wavelength, Standard IEC 60793-1-44, IEC subcommittee 86 A, London, U.K., 2011.

[54] C. R. Giles and E. Desurvire, "Modeling erbium-doped fiber amplifiers," *J. Lightw. Technol.*, vol. 9, no. 2, pp. 271–283, Feb. 1991.

[55] E. Desurvire, *Erbium-Doped Fiber Amplifiers: Principles and Applications*. Hoboken, NJ, USA: Wiley, 1994.

[56] P. S. Anisimov, V. S. Motolygin, V. V. Zemlyakov, and J. Gao, "Fast multi step-index mode solver for analysis and optimization of optical fiber performance," *J. Lightw. Technol.*, vol. 40, no. 9, pp. 2980–2987, May 2022.

[57] J.-B. Trinel, G. L. Cocq, Y. Quiquempois, E. R. Andresen, O. Vanvincq, and L. Bigot, "Theoretical study of gain-induced mode coupling and mode beating in few-mode optical fiber amplifiers," *Opt. Exp.*, vol. 25, no. 3, pp. 2377–2390, 2017.

[58] P. Pecci et al., "Pump farming as enabling factor to increase subsea cable capacity," in *Proc. SubOptic*, 2019, Paper OP14-4.

[59] J. D. Downie et al., "Experimental characterization of power efficiency for power-limited SDM submarine transmission systems," in *Proc. 46th Eur. Conf. Opt. Commun.*, 2020, pp. 1–4.

[60] K.-P. Ho and J. M. Kahn, "Mode-dependent loss and gain: Statistics and effect on mode-division multiplexing," *Opt. Exp.*, vol. 19, no. 17, pp. 16612–16635, Aug. 2011. [Online]. Available: http://opg.optica.org/oe/abstract.cfm?URI=oe-19-17-16612

[61] K. Choutagunta, S. O. Arik, K.-P. Ho, and J. M. Kahn, "Characterizing mode-dependent loss and gain in multimode components," *J. Lightw. Technol.*, vol. 36, no. 18, pp. 3815–3823, Sep. 2018.

[62] P. J. Winzer, H. Chen, R. Ryf, K. Guan, and S. Randel, "Mode-dependent loss, gain, and noise in MIMO-SDM systems," in *Proc. Eur. Conf. Opt. Commun.*, 2014, pp. 1–3.

[63] N. Riesen and J. D. Love, "Weakly-guiding mode-selective fiber couplers," *IEEE J. Quantum Electron.*, vol. 48, no. 7, pp. 941–945, Jul. 2012.

[64] K. Igarashi, K. J. Park, T. Tsuritani, I. Morita, and B. Y. Kim, "All-fiber-based selective mode multiplexer and demultiplexer for weakly-coupled mode-division multiplexed systems," *Opt. Commun.*, vol. 408, pp. 58–62, 2018. [Online]. Available: https://www.sciencedirect.com/science/article/pii/S003040181730737X

[65] K. Zhang et al., "Broadband mode-selective couplers based on tapered side-polished fibers," *Opt. Exp.*, vol. 29, no. 13, pp. 19690–19702, Jun. 2021. [Online]. Available: https://opg.optica.org/oe/abstract.cfm?URI=oe-29-13-19690

[66] S. H. Chang et al., "All-fiber 6-mode multiplexers based on fiber mode selective couplers," *Opt. Exp.*, vol. 25, no. 5, pp. 5734–5741, Mar. 2017. [Online]. Available: https://opg.optica.org/oe/abstract.cfm?URI=oe-25-5-5734

[67] I. Gasulla and J. M. Kahn, "Performance of direct-detection mode-group-division multiplexing using fused fiber couplers," *J. Lightw. Technol.*, vol. 33, no. 9, pp. 1748–1760, May 2015. [Online]. Available: https://opg.optica.org/jlt/abstract.cfm?URI=jlt-33-9-1748

[68] T. Wang et al., "High-order mode direct oscillation of few-mode fiber laser for high-quality cylindrical vector beams," *Opt. Exp.*, vol. 26, no. 9, pp. 11850–11858, Apr. 2018. [Online]. Available: https://opg.optica.org/oe/abstract.cfm?URI=oe-26-9-11850

[69] H. Guo, Y. ge Liu, H. Zhang, Z. Wang, and B. Mao, "980/1550 nm few-mode wavelength division multiplexing coupler based on a five-core fiber," *Opt. Commun.*, vol. 440, pp. 177–183, 2019. [Online]. Available: https://www.sciencedirect.com/science/article/pii/S0030401819300975

[70] J. D. Love and N. Riesen, "Mode-selective couplers for few-mode optical fiber networks," *Opt. Lett.*, vol. 37, no. 19, pp. 3990–3992, Oct. 2012. [Online]. Available: http://opg.optica.org/ol/abstract.cfm?URI=ol-37-19-3990

[71] S.-L. Chuang, "Application of the strongly coupled-mode theory to integrated optical devices," *IEEE J. Quantum Electron.*, vol. 23, no. 5, pp. 499–509, May 1987.

[72] CodeSeeder, "BeamLab," 2022. [Online]. Available: https://www.codeseeder.com/

[73] J. Meunier and S. Hosain, "An efficient model for splice loss evaluation in single-mode graded-index fibers," *J. Lightw. Technol.*, vol. 9, no. 11, pp. 1457–1463, Nov. 1991.

[74] H. Srinivas, E. S. Chou, D. A. A. Mello, K. Choutagunta, and J. M. Kahn, "Impact and mitigation of polarization- or mode-dependent gain in ultra-long-haul systems," in *Proc. 22nd Int. Conf. Transparent Opt. Netw.*, 2020, pp. 1–4.

[75] D. A. A. Mello, H. Srinivas, K. Choutagunta, R. S. B. Ospina, and J. M. Kahn, "Impact of mode-dependent gain on the capacity of ultra-long-haul SDM systems," in *Proc. IEEE Photon. Soc. Summer Topicals Meeting Ser.*, 2022, pp. 1–2.

[76] P. J. Winzer and G. J. Foschini, "MIMO capacities and outage probabilities in spatially multiplexed optical transport systems," *Opt. Exp.*, vol. 19, no. 17, pp. 16680–16696, Aug. 2011. [Online]. Available: https://opg.optica.org/oe/abstract.cfm?URI=oe-19-17-16680

[77] J. D. Downie, "Maximum capacities in submarine cables with fixed power constraints for C-band, C L-band, and multicore fiber systems," *J. Lightw. Technol.*, vol. 36, no. 18, pp. 4025–4032, Sep. 2018.

[78] A. Ellison and J. Minelly, "Chapter 3 - New materials for optical amplifiers," in *Opt. Fiber Telecommun. IV-A* (Series Optics and Photonics), 4th ed., I. P. Kaminow and T. Li, Eds. Burlington, ON, Canada: Academic, 2002, pp. 80–173. [Online]. Available: https://www.sciencedirect.com/science/article/pii/B9780123951724500036

[79] S. Unger, F. Lindner, C. Aichele, and K. Schuster, *Rare-Earth-Doped Laser Fiber Fabrication Using Vapor Deposition Technique*. Singapore:Springer, 2018 .

[80] Y. Chang et al., "Demonstration of an all-fiber cladding-pumped FM-EDFA with low differential modal gain," *Opt. Laser Technol.*, vol. 155, pp. 1–7, 2022, Art. no. 108446. [Online]. Available: https://www.sciencedirect.com/science/article/pii/S003039922200603X

[81] K. Anuar et al., "Er2O3-Al2O3 doped silica preform prepared by MCVD-chelate vapor phase delivery technique," *Adv. Mater. Res.*, vol. 896, pp. 219–224, 2014.

[82] D. S. Lipatov et al., "Fabrication and characterization of Er/Yb co-doped fluorophosphosilicate glass core optical fibers," *Fibers*, vol. 9, no. 3, 2021, Art. no. 15. [Online]. Available: https://www.mdpi.com/2079-6439/9/3/15

[83] N. Choudhury, N. K. Shekhar, A. Dhar, and R. Sen, "Graded-index ytterbium-doped optical fiber fabricated through vapor phase chelate delivery technique," *Physica Status Solidi (a)*, vol. 216, no. 20, 2019, Art. no. 1900365, doi: 10.1002/pssa.201900365.

[84] N. Choudhury et al., "Novel dopant tailored fibers using vapor phase chelate delivery technique," *Physica Status Solidi (a)*, vol. 219, no. 1, 2022, Art. no. 2100484, doi: 10.1002/pssa.202100484.

[85] T. Wang et al., "Efficient structural manipulation of PbS in Er-doped silica optical fibers for enhanced amplification systems," *J. Lumin.*, vol. 257, 2023, Art. no. 119689. [Online]. Available: https://www.sciencedirect.com/science/article/pii/S0022231323000224

[86] N. K. Fontaine et al., "Coupled-core optical amplifier," in *Proc. Opt. Fiber Commun. Conf. Postdeadline Papers*, 2017, Art. no. Th5D.3. [Online]. Available: http://opg.optica.org/abstract.cfm?URI=OFC-2017-Th5D.3

[87] D. W. Peckham, Y. Sun, A. McCurdy, and R. Lingle, "Chapter 8 - Few-mode fiber technology for spatial multiplexing," in *Opt. Fiber Telecommun.* (Series Optics and Photonics), 6th ed., I. P. Kaminow, T. Li, and A. E. Willner, Eds. Boston, MA, USA: Academic Press, 2013, pp. 283–319. [Online]. Available: https://www.sciencedirect.com/science/article/pii/B9780123969583000081

[88] D. Askarov and J. M. Kahn, "Long-period fiber gratings for mode coupling in mode-division-multiplexing systems," *J. Lightw. Technol.*, vol. 33, no. 19, pp. 4032–4038, Oct. 2015.

[89] Y. Liu, X. Wang, Z. Yang, L. Zhang, and G. Li, "Strongly coupled few-mode erbium-doped fiber amplifiers with ultralow differential modal gain," in *Proc. Opt. Fiber Commun. Conf.*, 2020, Paper W4B.7. [Online]. Available: http://opg.optica.org/abstract.cfm?URI=OFC-2020-W4B.7

[90] S. O. Arik, D. Askarov, and J. M. Kahn, "Effect of mode coupling on signal processing complexity in mode-division multiplexing," *J. Lightw. Technol.*, vol. 31, no. 3, pp. 423–431, Feb. 2013.

[91] K. S. Chiang and Q. Liu, "Long-period grating devices for application in optical communication," in *Proc. 5th Int. Conf. Opt. Commun. Netw.*, 2006, pp. 128–133.

[92] M. Wada, T. Sakamoto, T. Mori, T. Yamamoto, N. Hanzawa, and F. Yamamoto, "Modal gain controllable 2-LP-mode fiber amplifier using PLC type coupler and long-period grating," *J. Lightw. Technol.*, vol. 32, no. 24, pp. 4694–4700, Dec. 2014.

[93] S. O. Arik, K.-P. Ho, and J. M. Kahn, "Delay spread reduction in mode-division multiplexing: Mode coupling versus delay compensation," *J. Lightw. Technol.*, vol. 33, no. 21, pp. 4504–4512, Nov. 2015.

[94] S. O. Arik, K.-P. Ho, and J. M. Kahn, "Group delay management and multiinput multioutput signal processing in mode-division multiplexing systems," *J. Lightw. Technol.*, vol. 34, no. 11, pp. 2867–2880, Jun. 2016.

[95] T. Mori, T. Sakamoto, M. Wada, T. Yamamoto, and F. Yamamoto, "Low DMD four LP mode transmission fiber for wide-band WDM-MIMO system," in *Proc. Opt. Fiber Commun. Conf. Expo. Nat. Fiber Optic Engineers Conf.*, 2013, pp. 1–3.

[96] M. Grant and S. Boyd, "CVX: Matlab software for disciplined convex programming, Version 2.1," Mar. 2014. [Online]. Available: http://cvxr.com/cvx

[97] M. Grant and S. Boyd, "Graph Implementations for Nonsmooth Convex Programs," in *Recent Advances in Learning and Control* (Series Lecture Notes in Control and Information Sciences), V. Blondel, S. Boyd, and H. Kimura, Eds. Berlin, Germany: Springer, 2008, pp. 95–110.

[98] K.-P. Ho and J. M. Kahn, "Chapter 11 - Mode coupling and its impact on spatially multiplexed systems," in *Opt. Fiber Telecommun.* (Series Optics and Photonics), 6th ed., I. P. Kaminow, T. Li, and A. E. Willner, Eds. Boston, MA, USA: Academic, 2013, pp. 491–568. [Online]. Available: https://www.sciencedirect.com/science/article/pii/B9780123969606000110

[99] K.-P. Ho and J. M. Kahn, "Delay-spread distribution for multimode fiber with strong mode coupling," *IEEE Photon. Technol. Lett.*, vol. 24, no. 21, pp. 1906–1909, Nov. 2012.

[100] B. Baeuerle, A. Josten, M. Eppenberger, D. Hillerkuss, and J. Leuthold, "Low-complexity real-time receiver for coherent Nyquist-FDM signals," *J. Lightw. Technol.*, vol. 36, no. 24, pp. 5728–5737, Dec. 2018.

[101] S. O. Arik, D. Askarov, and J. M. Kahn, "Adaptive frequency-domain equalization in mode-division multiplexing systems," *J. Lightw. Technol.*, vol. 32, no. 10, pp. 1841–1852, May 2014. [Online]. Available: https://opg.optica.org/jlt/abstract.cfm?URI=jlt-32-10-1841

[102] K. Choutagunta, I. Roberts, and J. M. Kahn, "Efficient quantification and simulation of modal dynamics in multimode fiber links," *J. Lightw. Technol.*, vol. 37, no. 8, pp. 1813–1825, Apr. 2019.

Hrishikesh Srinivas (Member, IEEE) received the B.E. degree in photonic engineering and the B.Sc. degree in mathematics and physical science from the University of New South Wales, Sydney, NSW, Australia, and the M.S. and Ph.D. degrees in electrical engineering from Stanford University, Stanford, CA, USA. His research interests include optical communications, optical amplifier physics, and photonics.

Oleksiy Krutko received the B.S. degree in electrical engineering from the University of Texas at Austin, Austin, TX, USA, in 2020. He is currently working toward the Ph.D. degree from Stanford University, Stanford, CA, USA. His research interests include optical fiber communications and photonic devices.

Joseph M. Kahn (Fellow, IEEE) received the A.B., M.A., and Ph.D. degrees in physics from the University of California, Berkeley, CA, USA, in 1981, 1983 and 1986. From 1987to 1990, he was with AT&T Bell Laboratories. In 1989, he demonstrated the first successful synchronous (i.e., coherent) detection using semiconductor lasers, achieving record receiver sensitivity. From 1990 to 2003, he was on the Electrical Engineering and Computer Sciences Faculty, Berkeley. He demonstrated coherent detection of QPSK in 1992. In 1999, D.-S. Shiu and Kahn published the first work on probabilistic shaping for optical communications. In the 1990s and early 2000s, Kahn and collaborators performed seminal work on indoor and outdoor free-space optical communications and multi-input multi-output wireless communications. In 2000, Kahn and K.-P. Ho founded StrataLight Communications, whose 40 Gb/s-per-wavelength long-haul fiber transmission systems were deployed widely by AT&T, Deutsche Telekom, and other carriers. In 2002, Ho and Kahn applied to patent the first electronic compensation of fiber Kerr nonlinearity. StrataLight was acquired by Opnext in 2009. In 2003, he became a Professor of electrical engineering with E. L. Ginzton Laboratory, Stanford University, Stanford, CA, USA. Kahn and collaborators have extensively studied rate-adaptive coding and modulation, and digital signal processing for mitigating linear and nonlinear impairments in coherent systems. In 2008, E. Ip and Kahn (and G. Li independently) invented simplified digital backpropagation for compensating fiber Kerr nonlinearity and dispersion. Since 2004, Kahn and collaborators has been studying propagation, modal statistics, spatial multiplexing and imaging in multi-mode fibers, elucidating principal modes and demonstrating transmission beyond the traditional bandwidth-distance limit in 2005, deriving the statistics of coupled modal group delays and gains in 2011, and deriving resolution limits for imaging in 2013. His research addresses optical frequency comb generators, coherent data center links, rate-adaptive access networks, fiber Kerr nonlinearity mitigation, ultra-long-haul submarine links, and optimal free-space transmission through atmospheric turbulence. Kahn was the recipient of the National Science Foundation Presidential Young Investigator Award in 1991. In 2000, he became a Fellow of the IEEE.